RESEARCH ARTICLE

National Science Review
9: nwab225, 2022
https://doi.org/10.1093/nsr/nwab225
Advance access publication 15 December 2021

PHYSICS

Direct observation of nodeless superconductivity and phonon modes in electron-doped copper oxide $Sr_{1-x}Nd_xCuO_2$

Jia-Qi Fan[1], Xue-Qing Yu[1], Fang-Jun Cheng[1], Heng Wang[1], Ruifeng Wang[1], Xiaobing Ma[1], Xiao-Peng Hu[1], Ding Zhang[1,2,3,4], Xu-Cun Ma[1,2,*], Qi-Kun Xue[1,2,3,5,*] and Can-Li Song[1,2,*]

[1]State Key Laboratory of Low-Dimensional Quantum Physics, Department of Physics, Tsinghua University, Beijing 100084, China; [2]Frontier Science Center for Quantum Information, Beijing 100084, China; [3]Beijing Academy of Quantum Information Sciences, Beijing 100193, China; [4]RIKEN Center for Emergent Matter Science (CEMS), Wako, Saitama 351-0198, Japan and [5]Southern University of Science and Technology, Shenzhen 518055, China

***Corresponding authors.** E-mails: clsong07@mail.tsinghua.edu.cn; xucunma@mail.tsinghua.edu.cn; qkxue@mail.tsinghua.edu.cn

Received 3 July 2021; **Revised** 10 December 2021; **Accepted** 12 December 2021

ABSTRACT

The microscopic understanding of high-temperature superconductivity in cuprates has been hindered by the apparent complexity of crystal structures in these materials. We used scanning tunneling microscopy and spectroscopy to study the electron-doped copper oxide compound $Sr_{1-x}Nd_xCuO_2$, which has only bare cations separating the CuO_2 planes and thus the simplest infinite-layer structure of all cuprate superconductors. Tunneling conductance spectra of the major CuO_2 planes in the superconducting state revealed direct evidence for a nodeless pairing gap, regardless of variation of its magnitude with the local doping of trivalent neodymium. Furthermore, three distinct bosonic modes are observed as multiple peak-dip-hump features outside the superconducting gaps and their respective energies depend little on the spatially varying gaps. As well as the bosonic modes, with energies identical to those of the external, bending and stretching phonons of copper oxides, our findings reveal the origin of the bosonic modes in lattice vibrations rather than spin excitations.

Keywords: nodeless superconductivity, phonon modes, cuprate superconductors, CuO_2 plane

INTRODUCTION

Despite more than three decades of intensive research, it remains a mystery how high-temperature (T_c) superconductivity works in a family of ceramic materials known as cuprates [1,2]. In pursuit of its microscopic mechanism, two fundamental prerequisites are needed to identify the superconducting energy gap (Δ) function and bosonic glue (e.g. lattice vibrations and spin excitations) to pair electrons of the copper oxide (CuO_2) planes. In theory [3], the bosonic excitation (mode) often exhibits itself via a strong coupling to the paired electrons, in the low-lying quasiparticle states at energy $E = \Delta + \Omega$ (Ω is the boson energy). This shows great promise for simultaneously measuring the Δ and Ω by tunneling spectroscopy, which has unequivocally established the phonon-mediated *s*-wave pairing state in conventional superconductors [4]. For cuprate superconductors, however, no consensus exists on both the superconducting gap symmetry and the pairing glue [2,5–12]. One explanation could be that previous tunneling data from surface-sensitive scanning tunneling microscopy (STM) have been mostly measured on various charge reservoir layers [8,10–12], where a nodal gap behavior probably associated with charge density wave often occurs [2,13]. Here we report a high-resolution STM study of the electron-doped cuprate compound $Sr_{1-x}Nd_xCuO_2$ (SNCO, $x \sim 0.100$) and directly reveal nodeless superconductivity and three distinct bosonic modes on the CuO_2 planes. Our analysis of the bosonic mode energies, which depend little on the spatially varying Δ, supports a lattice vibrational origin of the modes consistent with external, bending and stretching phonons of the copper oxides.

Infinite-layer $SrCuO_2$ is, structurally, one of the simplest cuprate parent compounds that comprises

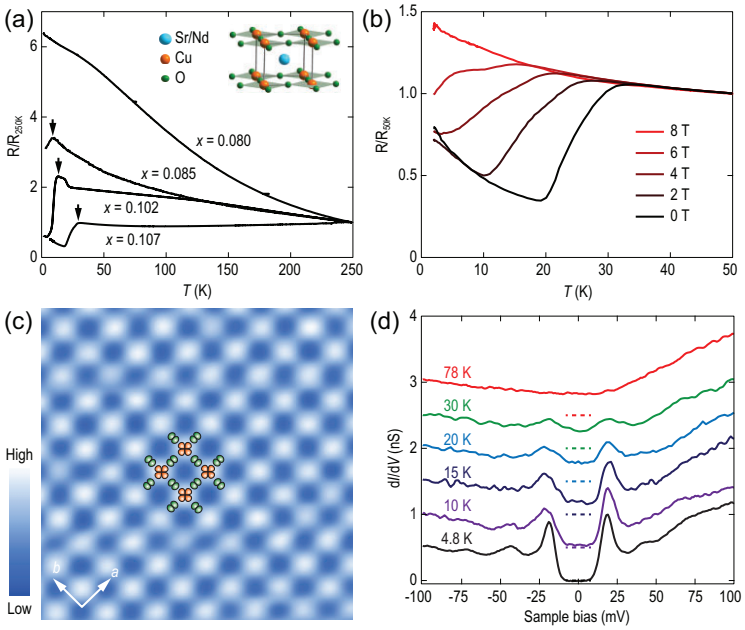

Figure 1. Characterizations of SNCO epitaxial films. (a) Temperature dependence of electrical resistivity, normalized to the value of 250 K, in electron-doped $Sr_{1-x}Nd_xCuO_2$ ($0.080 \leq x \leq 0.107$) cuprate films, with a nominal thickness of ∼13 nm. Arrows denote the onset temperatures of superconductivity. Inset shows the schematic crystal structure of SNCO. (b) Electrical resistivity versus temperature of $Sr_{0.893}Nd_{0.107}CuO_2$ measured under different magnetic fields, normalized to the value of 50 K for clarification. (c) Atom-resolution STM topography (3.6 nm × 3.6 nm, $V = -1.5$ V, $I = 20$ pA) of $x \sim 0.100$ SNCO film. The bright spots denote the Cu atoms at the top layer. A single CuO_2 plaquette with Cu 3d (orange) and O 2p (green) orbitals is shown. (d) Temperature dependence of differential conductance d*I*/d*V* spectra on the superconducting CuO_2 plane. Setpoint: $V = -200$ mV and $I = 100$ pA.

the essential CuO_2 planes separated only by strontium atoms. Partial substitution of divalent strontium (Sr^{2+}) by trivalent neodymium (Nd^{3+}) ions leads to electron doping and superconductivity with a record electron-doped cuprate transition temperature T_c of 40 K [14]. Most importantly, the single-crystalline SNCO epitaxial films with well-controlled doping level x, grown on $SrTiO_3(001)$ substrates with an oxide molecular beam epitaxy (MBE), exhibit a rare surface termination of the essential CuO_2 planes [15–17]. Tunneling spectra of the electron-doped infinite-layer cuprates, which have so far been largely unexplored compared to their hole-doped counterparts [8], pose considerable challenges and opportunities. The challenge is to clarify whether the electron-doped cuprates and direct measurements of the major CuO_2 planes are fundamentally different from or analogous to their hole-doped counterparts and those of the charge reservoir planes, respectively, whereas the critical opportunity is that addressing these issues might help greatly in finding the culprit of high-T_c superconductivity in copper oxide superconductors.

RESULTS

Temperature-dependent resistivity in $Sr_{1-x}Nd_xCuO_2$

Figure 1a plots the temperature dependence of the electrical resistivity of SNCO with varying Nd doping concentration x. An insulator–superconductor transition triggered by Nd^{3+} dopants becomes evident at $x > 0.080$. The superconducting phase is further unambiguously confirmed by applying an external magnetic field to the $x = 0.107$ SNCO sample in Fig. 1b. As anticipated, the electrical resistivity at low temperatures is elevated with increasing field until a complete suppression of superconductivity at 8 T. It is worth noting that the resistivity does not drop down to zero below T_c. Instead, it exhibits an upturn behavior, which is later revealed by site-resolved tunneling spectroscopy to arise from nanoscale electronic phase separation between the superconductivity and under-doped Mott insulating state. Anyhow, the observed T_c onset (marked by the black arrows in Fig. 1a) up to 30 K turns out to be higher than those previously reported in epitaxial SNCO films on $SrTiO_3$ substrates [18].

Spectroscopic evidence of nodeless superconductivity and phonon modes

As demonstrated before [15–17], the heteroepitaxy of SNCO films on $SrTiO_3$ proceeds in a typical layer-by-layer mode. Figure 1c shows a constant-current STM topographic image that displays an atomically flat and defect-free copper oxide surface in one SNCO sample of $x \sim 0.100$. The adjacent Cu atoms are spaced ∼0.39 nm apart, which agrees with the previous reports [14–17]. In Fig. 1d, we show the energy-resolved tunneling conductance (dI/dV) spectra, being proportional to the quasiparticle density of states (DOS), directly on the CuO_2 plane. At 4.8 K, the spectral weight is completely removed over a finite energy range around the Fermi level (E_F), and instead considerable DOS piles up at two E_F-symmetric gap edges of about ±19 meV. These characteristics, hallmarks of fully gapped superconductivity, suggest no gap node in the superconducting gap function of SNCO on the Fermi surface. At elevated temperatures, the superconducting gap is progressively smeared out and vanishes at 78 K (see the red curve). Note that, albeit weak (green curve), the gap survives above the observed T_c maximum of ∼30 K as shown in the electrical transport measurements in Fig. 1a, which we here ascribe to a spatial inhomogeneity of T_c inside the SNCO films.

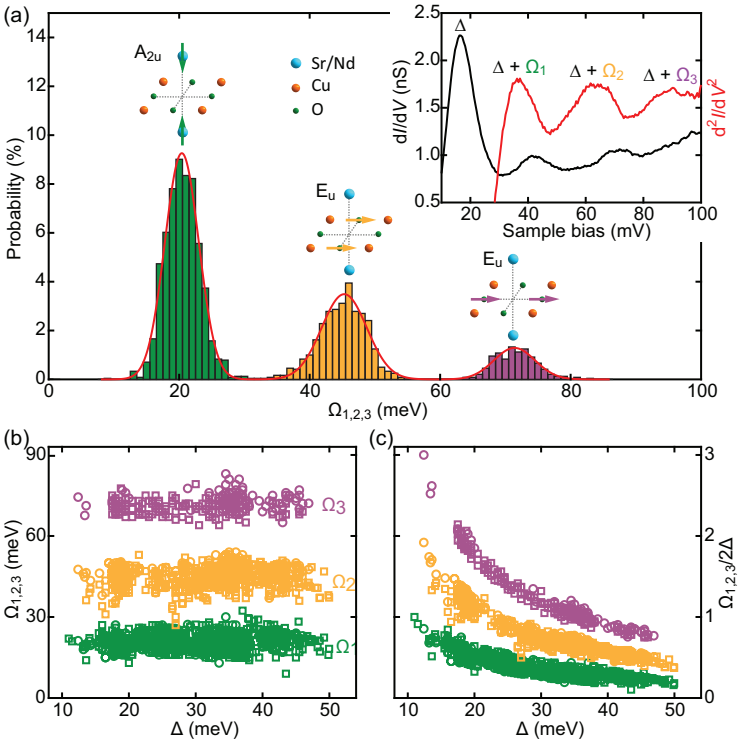

Figure 2. Lattice vibrational modes. (a) Histogram of measured bosonic mode energies Ω from a sequence of d*I*/d*V* spectra in nine similar SNCO samples with $x \sim 0.10$. By fitting the data to a multipeak Gaussian function, three distinct bosonic modes at $\Omega_1 = 20 \pm 3$ meV, $\Omega_2 = 45 \pm 4$ meV and $\Omega_3 = 72 \pm 3$ meV are obtained, with their energies close to those of the external (green arrows), bending (yellow arrows) and stretching (purple arrows) phonons of copper oxides [22,23]. Here the statistical errors of $\Omega_{1,2,3}$ indicate the full width at half maximum of the corresponding Gaussian peaks. Inserted in the top right corner are a representative superconducting spectrum (setpoint: $V = -200$ mV and $I = 100$ pA) and its derivative in the empty states, from which $\Omega_{1,2,3}$ can be readily extracted. (b) and (c) Variation of the bosonic mode energies $\Omega_{1,2,3}$ and $\Omega_{1,2,3}/2\Delta$ with the spatially varying gap magnitude Δ. Two different symbols of circles and squares denote data extracted from the occupied and empty states, respectively.

Careful measurements on various samples and superconducting regions indicate that the nodeless electron pairing occurs universally on the CuO_2 planes of SNCO, irrespective of the spatial inhomogeneity in Δ (Figs S1 and S2 in the online supplementary material). This finding turns out to be consistent with previous tunneling and angle-resolved photoemission studies of a sister compound $Sr_{0.9}La_{0.1}CuO_2$ [19,20]. Furthermore, multiple peak-dip-hump fine structures develop frequently (>75%) outside the superconducting gaps, which are pairwise centered at E_F and smear out at elevated temperatures (Fig. 1d). These traits were commonly interpreted as the signatures of bosonic excitations in superconductors [4,10–12]. Tunneling spectra on the bosonic mode energy Ω and its correlation with Δ can potentially distinguish between candidates for the pairing glue [10–12,21]. Inserted in Fig. 2a are one representative superconducting spectrum (black curve) and its derivative (d^2I/dV^2, red curve), only showing the empty states. By taking the maxima in the second derivative of conductance d^2I/dV^2 as estimates of the energies $E = \Delta + \Omega$, three bosonic modes with energies at $\Omega_{1,2,3}$ are extracted. A statistical estimate of Ω from all measured superconducting dI/dV spectra in both empty and occupied states yields thousands of independent observables, whose histograms are plotted in Fig. 2a. The average mode energies are measured to be $\Omega_1 = 20 \pm 3$ meV, $\Omega_2 = 45 \pm 4$ meV and $\Omega_3 = 72 \pm 3$ meV, respectively. Evidently, Ω_2 and Ω_3 are not multiples of Ω_1 (Fig. S3 in the online supplementary material), which excludes the possibility that they are caused by a harmonic multi-boson excitation of the same mode Ω_1. This appears to be in good agreement with the intensity differences of $\Omega_{1,2,3}$ (Fig. 1d, and Fig. S1 in the online supplementary material). For some spectra, the bosonic modes Ω_2 and Ω_3 are too faint to be easily read out, leading to their probabilities being relatively lower than Ω_1 in the histograms of $\Omega_{1,2,3}$ (Fig. 2a).

The correlations between the spatially resolved $\Omega_{1,2,3}$ and Δ are plotted in Fig. 2b and c. Despite a substantial spatial variation in Δ (Fig. S2 in the online supplementary material), the bosonic mode energies $\Omega_{1,2,3}$ alter little and the local ratio of $\Omega_{1,2,3}$ to 2Δ ($\Omega_{1,2,3}/2\Delta$) exceeds unity for small Δ. Both findings run counter to the scenario of spin excitations, whose energies are generally dependent on Δ [11] and remain below the pair-breaking energy, to wit, $\Omega/2\Delta < 1$ [21]. By contrast, since energies of lattice vibrations change little with the doping level (i.e. Δ), they are natural candidates for the three bosonic excitations observed. Actually, the $\Omega_{1,2,3}$ show incredible coincidences with the external (∼20 meV), bending (∼45 meV) and stretching (∼72 meV) phonon mode energies, which were measured independently by optics [22] and Raman [23] in bulk $SrCuO_2$. It should be stressed that this concurrent observation of the three key phonon modes from one spectrum is rather challenging in cuprate superconductors. We attribute this unprecedented success to a rare new measure of the major CuO_2 planes.

Nanoscale electronic phase separation

To eliminate any possible artifacts in our measurements, we collected spatially resolved tunneling dI/dV spectra over many regions of the samples and checked the tunneling junction quality. A representative set of dI/dV spectra in the superconducting region exhibit superior robustness of the nodeless pairing, coherence peaks and peak-dip-hump

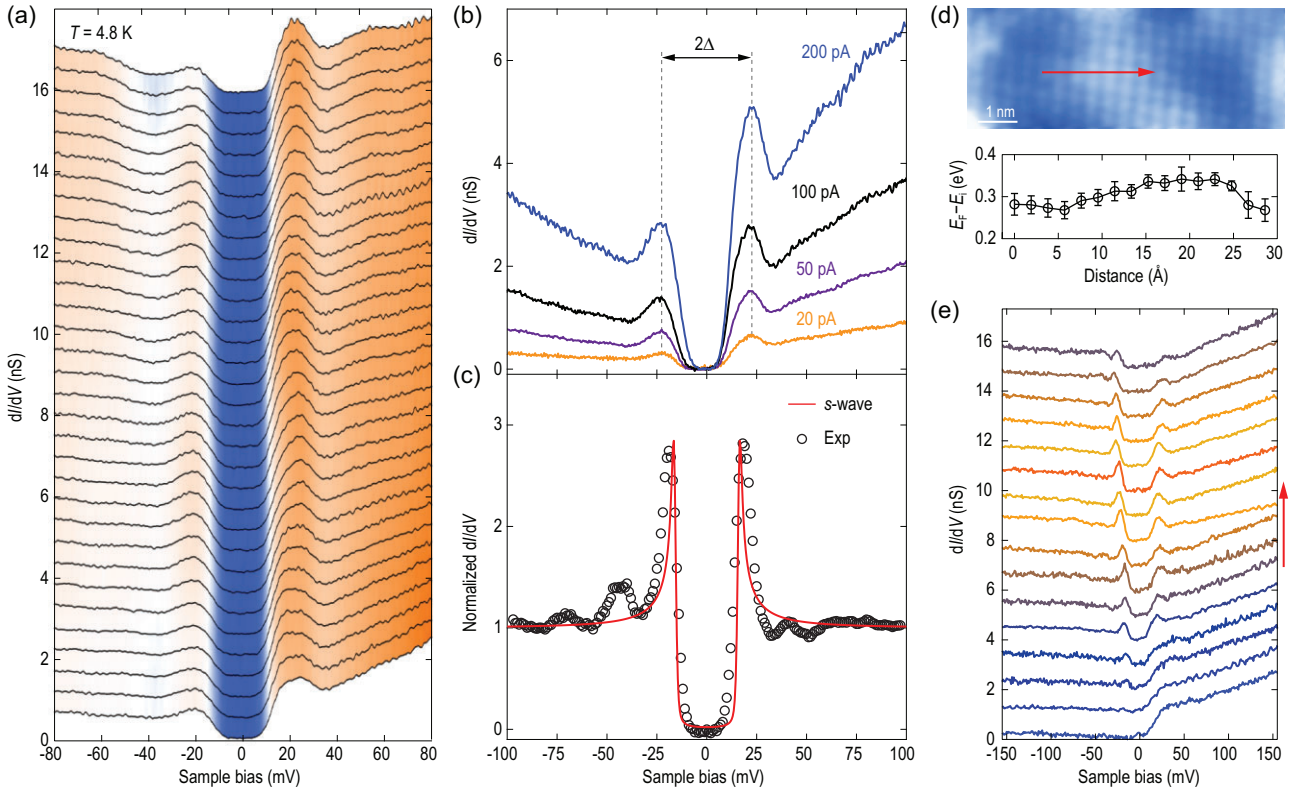

Figure 3. Tunneling spectra and nodeless superconductivity on CuO_2. (a) Line-cut d*I*/d*V* spectra taken at equal separations (0.05 nm) in one superconducting domain. Setpoint: $V = -100$ mV and $I = 100$ pA. (b) Tip-to-sample distance dependence of d*I*/d*V* spectra at a specific position. The tunneling current I is changed from 20 pA (large distance, bottom curve) to 200 pA (small distance, top curve) at a constantly stabilized $V = -100$ mV. (c) Normalized d*I*/d*V* spectrum with pronounced coherence peaks at 4.8 K (circles) and its best fit (red curve) to a single *s*-wave superconducting gap with $\Delta = 17$ meV. The normalization was performed by dividing the raw d*I*/d*V* spectrum by its background, which was extracted from a quadratic fit to the conductance for $|V| > 50$ mV. (d) An 8 nm × 3 nm STM topography ($V = -1.0$ V, $I = 20$ pA) showing nanoscale phase separation between superconducting (bright) and insulating (dark) domains. The bottom panel shows E_F shifts relative to E_i along the red arrow. Here a larger $E_F - E_i$ means heavier electron doping. (e) A series of d*I*/d*V* spectra acquired along the red arrow in (d), plotted from bottom to top. Setpoint: $V = 200$ mV and $I = 100$ pA.

line shapes (Fig. 3a). Figure 3b compares a series of site-specific dI/dV spectra taken as a function of increasing the tip-to-sample distance (from top to bottom). The full superconducting gap remains essentially unchanged at any tunneling current, as anticipated for ideal vacuum tunneling. It was also found that a fraction of superconducting gaps display pronounced coherence peaks and could be fitted by the Dynes model using a single *s*-wave gap function [24], as exemplified in Fig. 3c. A minor discrepancy occurs between measured (black circles) and fitted (red curve) curves in the superconducting gap and suggests excess subgap DOS, whose origin merits further study. Figure 3d exhibits another region in which a set of spatially dependent dI/dV spectra (Fig. 3e) were taken along the red arrow. Note that the atomically resolved STM topography of Fig. 3d was acquired at −1.0 V, just around the charge-transfer band (CTB) onset of CuO_2 in the electron-doped SNCO films [16,17]. The STM contrast mainly has an electronic origin (Fig. S4 in the online supplementary material). Domains mapped as bright correspond to the regions with relatively heavier neodymium dopants and thereby more emergent in-gap states (IGSs), and vice versa [16,25]. A local measurement of E_F relative to the midgap energy E_i (i.e. the center of charge transfer gap) of CuO_2 [16], by exploring the spatial dependence of wider-energy-ranged dI/dV spectra in Fig. S5, convincingly supports this claim. As verified in the bottom panel of Fig. 3d, the $E_F - E_i$ value, a good indicator of the electron doping level of neodymium, appears to be larger in the bright regions than in the dark ones. Meanwhile, a crossover from the full superconducting gaps to gapless or somewhat insulating tunneling spectra is apparent as the STM tip moves from the bright regions to the dark ones (Fig. 3e). Such direct imaging of the nanoscale electronic phase separation, which proves the existence of a generic characteristic of the SNCO epitaxial films (Fig. S2 in the online supplementary material) and has been extensively documented in

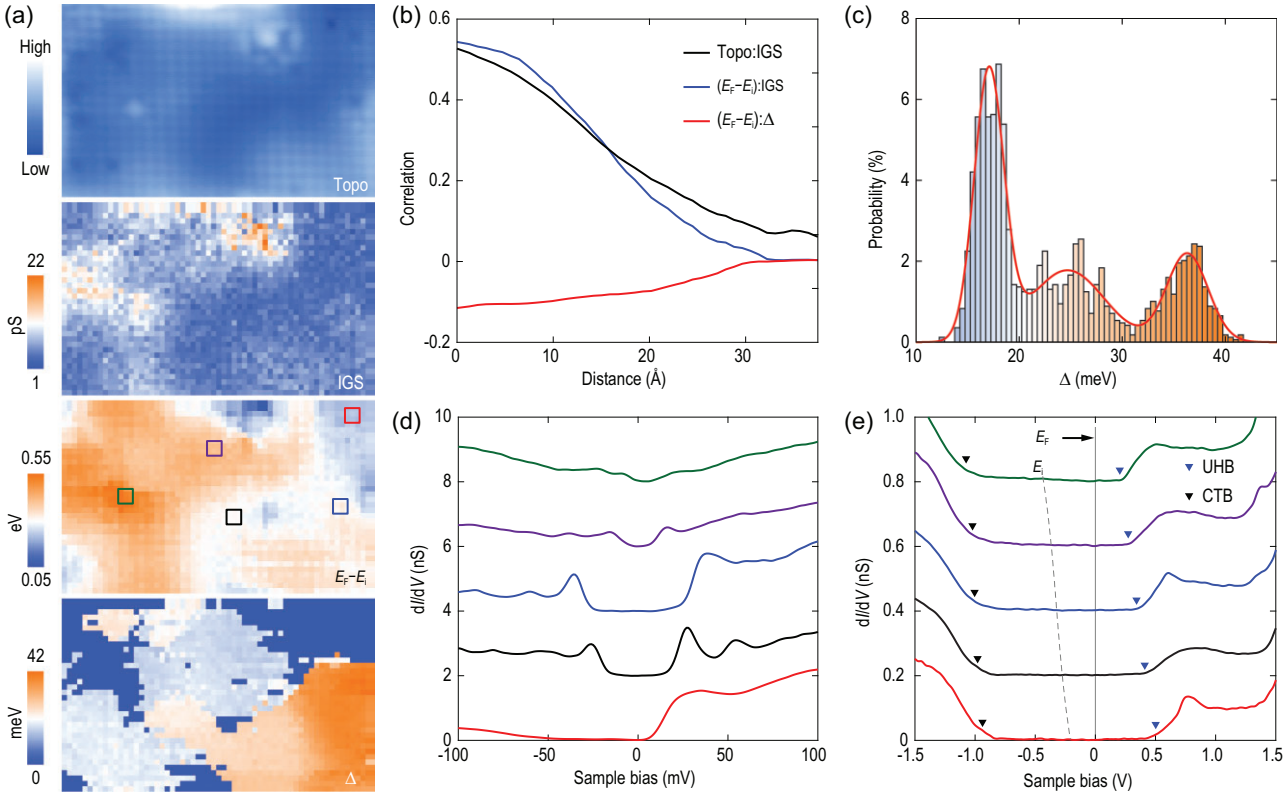

Figure 4. Spectroscopic mapping of nanoscale electronic phase separation. (a) Topography (10.5 nm × 6.2 nm, $V = -0.8$ V, $I = 20$ pA), spatial maps of IGSs, $E_F - E_i$ and Δ extracted from a grid (61 pixels × 36 pixels) of spectroscopic data over the same field of view. The STM tip is stabilized at $V = -1.6$ V, $I = 100$ pA and $V = -200$ mV, $I = 100$ pA to measure the dI/dV spectra in the wide and narrow voltage ranges, respectively. (b) Angle-averaged cross-correlations of IGSs with the STM topography (black) and $E_F - E_i$ (blue), as well as cross-correlation between the Δ and $E_F - E_i$ (red). (c) Histogram of the superconducting gap Δ. Three discrete peaks from the multipeak Gaussian fit (red) arise from various superconducting domains with different doping levels. (d) and (e) Spatially averaged dI/dV spectra on the square-marked regions in the second lowest panel of (a), color coded to match with each other, measured in both narrow and wide energy scale ranges, respectively. The dashed line tracks the evolution of E_i, which evenly separates between the CTB (black triangles) and upper-Hubbard band (UHB, blue triangles) of the CuO_2 plane, while the gray solid line denotes E_F.

other copper oxide superconductors [26,27], offers a straightforward account for the unusual electrical resistivity behavior in Fig. 1a and b.

In order to cast more light on the superconductivity of CuO_2 at the nanoscale, we further mapped dI/dV spectra in both wide (from −1.5 to 1.5 V) and narrow (from −200 mV to 200 mV) voltage ranges, from which the local doping level and Δ can be readily extracted and compared in the same field of view. Data from such maps are shown in Fig. 4a. Here the spatial IGSs are estimated by integrating the spectral weights within the charge-transfer gap of the CuO_2 plane, while the Δ is defined as half the separation between the two E_F-symmetric superconducting coherence peaks. A direct visual comparison between the corresponding maps in Fig. 4a, and their cross-correlation in Fig. 4b, reveals that the larger $E_F - E_i$ is correlated with topographically bright regions of populated IGSs on a short-length scale of ∼3 nm. By contrast, the correlation between the $E_F - E_i$ value and Δ is too small to draw any unbiased opinion. A careful inspection shows a strong spatial inhomogeneity of Δ (Fig. 4c) that relies non-monotonically on the $E_F - E_i$ value (Fig. 4d and e). The superconducting gap emerges at a certain threshold of $E_F - E_i$ (i.e. the electron doping level), increases and then decreases in magnitude as the local doping level is increased further. This describes a primary source of the weak correlation between them (Fig. 4b). Such a non-monotonic variation of Δ with the local doping level is derived from one sample by taking advantage of the dopant-induced nanoscale electronic inhomogeneity and differs from the nodal *d*-wave gap behavior previously reported on the charge reservoir planes [2,8], which declines linearly with the chemical doping. Instead, it bears a resemblance to the dome-shaped (T_c versus doping) superconducting phase diagram of both electron- and hole-doped cuprates [1,2,28,29]. This indicates that the observed nodeless gaps on the CuO_2 plane are intimately linked to the superconducting properties (T_c) of cuprates.

CONCLUSION

We have arrived at our key findings of superconducting CuO_2 planes in SNCO, namely the nodeless electron pairing and spectroscopic evidence for the lattice vibrational modes in the superconducting domains. Although the $E_F - E_i$ and Δ vary significantly from domain to domain, the superconducting gaps are always fully opened on the Fermi surface (Figs 3 and 4d, and Figs S1 and S2 in the online supplementary material). A statistical average of Δ from >3400 dI/dV spectra over many superconducting domains of all nine SNCO samples we studied (Fig. S1 in the online supplementary material) yields a value of 27 $\pm$ 8 meV. This mean gap size and the maximum gap $\Delta_{max} \sim 40$ meV observed in Fig. 4c stand out as the highest of records in all electron-doped cuprate superconductors [19,20,28], and are comparable to those reported in the hole-doped counterparts [29]. Under this context, equivalently high-T_c superconductivity might be potentially realized in the electron-doped infinite-layer cuprates once the inherent sample inhomogeneity is best minimized [30].

Our direct observation of nodeless superconductivity in the electron-doped cuprates of SNCO differs from the prior STM probe of a nodal *d*-wave gap function on the charge reservoir planes of various hole-doped cuprates [8]. Although it is tempting to examine the effect of an antiferromagnetic order on the nodeless energy gaps [20,31], our results exhibit much better consistency with those on the superconducting CuO_2 planes [9,32,33]. It thus becomes highly desirable to revisit the role of charge reservoir layers during tunneling measurements of cuprates, and to find out whether the nodeless electron pairing is generic to the CuO_2 planes of the copper oxide superconductors. Combined with the simultaneous measurements of lattice vibrational modes, which are indiscernible from tunneling spectra of the non-superconducting domains due to the vanishing paired electrons there (Fig. 4d), our results agree with a phonon-mediated *s*-wave pairing state in SNCO. However, caution is taken when explaining the findings using the conventional wisdom of Bardeen-Cooper-Schrieffer (BCS) theory. This is because of (i) the gap-to-T_c ratio $2\Delta/k_BT_c \sim 14$ (Fig. 1d) that largely exceeds the weak-coupling BCS value of 3.53 and (ii) the anomalous dome-shaped doping dependence of Δ (BCS theory predicts no obvious dependence of Δ on doping). These unconventional features, which have been observed in fulleride superconductors [34] and monolayer FeSe films grown on $SrTiO_3(001)$ substrates [35–37], go beyond the weak-coupling BCS picture. They do not, however, necessarily violate a phonon-mediated superconducting state with the local non-retarded pairs [38]. From this point of view, our results demonstrate the vital significance of electron-lattice interaction in the superconductivity of infinite-layer cuprates [39]. A further measurement of the oxygen isotope effects on Δ and Ω helps understand the role of phonons in the observed nodeless superconductivity.

MATERIALS AND METHODS

Sample growth

High-quality SNCO ($0.008 < x < 0.110$) thin films were epitaxially grown in an ozone-assisted molecular beam epitaxy (O-MBE) chamber that contained a quartz crystal microbalance (QCM, Inficon SQM160H) for precise flux calibration. Atomically flat $SrTiO_3(001)$ substrates with different Nb doping levels of 0.05 wt% and 0.5 wt% were heated to 1200°C under ultra-high vacuum (UHV) conditions for 20 minutes to acquire a TiO_2 terminated surface. The epitaxial SNCO films for STM and transport measurements were prepared on the 0.5 wt% and 0.05 wt% Nb-doped $SrTiO_3$ substrates, respectively. As oxidant, the distilled ozone flux was injected from a home-built ozone system into the O-MBE chamber by a nozzle, ~40 mm away from the substrates. All samples were grown by co-evaporating high-purity metal sources (Nd, Sr and Cu) from standard Knudsen cells under an ozone beam flux of $\sim 1.1 \times 10^{-5}$ Torr and at an optimized substrate temperature T_{sub} of 550°C [17]. The lower T_{sub} (<500°C) was revealed to degrade the sample quality of SNCO severely, while the higher ones (>610°C) resulted in another competing orthorhombic phase. After growth, the films were annealed in UHV at the identical T_{sub} for 0.5 hours and then cooled down to room temperature.

Prior to every film growth, we calibrated the beam flux of metal sources in sequence, to ensure the stoichiometry of SNCO films. The growth rate was kept at ~0.4 unit cells per minute. The doping level x was nominally deduced by *in-situ* QCM by calculating the flux ratio between the Nd and Cu sources, with an experimental uncertainty of ~0.5%. At the same time, the satellite peaks (Kiessig fringes) in the X-ray diffraction (XRD) spectra allowed us to estimate the film thickness [16,17], which agreed nicely with the nominal one deduced by the QCM-measured flux of Cu and growth duration.

In-situ STM measurements

All STM measurements were performed in a Unisoku USM 1300S ^{3}He system, which was

connected to the O-MBE chamber, at a constant temperature of 4.8 K, unless otherwise specified. The system pressure was lower than 1.0×10^{-10} Torr. Polycrystalline PtIr tips were cleaned via *e*-beam bombardment and calibrated on MBE-prepared Ag/Si(111) prior to the STM measurements. The STM topographies were acquired in a constant current mode with the voltage applied on the sample. The differential conductance dI/dV spectra and maps were measured by using a standard lock-in technique with a small bias modulation at 937 Hz. The system grounding and shielding were optimized to increase the stability and spectroscopic energy resolution ($\sim$1.0 meV) of our STM apparatus.

Transport measurements

After *in-situ* STM characterization and *ex-situ* XRD measurements, the transport measurements were carried out in a standard physical property measurement system (PPMS, Quantum Design). Freshly cut indium dots were cold pressed onto the samples as contacts. The resistivity was measured in a four-terminal configuration by a standard lock-in technique with a typical excitation current of 1 μA at 13 Hz.

SUPPLEMENTARY DATA

Supplementary data are available at *NSR* online.

FUNDING

This work was supported by the National Natural Science Foundation of China (51788104, 11634007, 11774192 and 11790311) and the Ministry of Science and Technology of China (2018YFA0305603, 2017YFA0304600 and 2017YFA0302902).

AUTHOR CONTRIBUTIONS

C.L.S., X.C.M. and Q.K.X. conceived the project; J.Q.F., X.Q.Y. and F.J.C. synthesized the thin film samples and performed the STM experiments with assistance from X.P.H.; H.W. and D.Z. carried out the transport measurements; J.Q.F. analyzed the data with assistance from X.Q.Y., F.J.C., R.F.W. and X.B.M.; C.L.S. and J.Q.F. wrote the manuscript with input from D.Z., X.C.M. and Q.K.X.; and all authors discussed the results and commented on the manuscript.

Conflict of interest statement. None declared.

REFERENCES

1. Keimer B, Kivelson SA and Norman MR *et al.* From quantum matter to high-temperature superconductivity in copper oxides. *Nature* 2015; **518**: 179–86.
2. Stewart GR. Unconventional superconductivity. *Adv Phys* 2017; **66**: 75–196.
3. Carbotte JP. Properties of boson-exchange superconductors. *Rev Mod Phys* 1990; **62**: 1027–157.
4. McMillan WL and Rowell JM. Lead phonon spectrum calculated from superconducting density of states. *Phys Rev Lett* 1965; **14**: 108–12.
5. Li Q, Tsay YN and Suenaga M *et al.* $Bi_2Sr_2CaCu_2O_{8+\delta}$ bicrystal *c*-axis twist Josephson junctions: a new phase-sensitive test of order parameter symmetry. *Phys Rev Lett* 1999; **83**: 4160–3.
6. Tsuei CC and Kirtley JR. Pairing symmetry in cuprate superconductors. *Rev Mod Phys* 2000; **72**: 969–1016.
7. Zhu YY, Liao M and Zhang Q *et al.* Presence of *s*-wave pairing in Josephson junctions made of twisted ultrathin $Bi_2Sr_2CaCu_2O_{8+x}$ flakes. *Phys Rev X* 2021; **11**: 031001.
8. Fischer Ø, Kugler M and Maggio-Aprile I *et al.* Scanning tunneling spectroscopy of high-temperature superconductors. *Rev Mod Phys* 2007; **79**: 353–419.
9. Zhong Y, Wang Y and Han S *et al.* Nodeless pairing in superconducting copper-oxide monolayer films on $Bi_2Sr_2CaCu_2O_{8+\delta}$. *Sci Bull* 2016; **61**: 1239–47.
10. Lee J, Fujita K and McElroy K *et al.* Interplay of electron-lattice interactions and superconductivity in $Bi_2Sr_2CaCu_2O_{8+\delta}$. *Nature* 2006; **442**: 546–50.
11. Niestemski FC, Kunwar S and Zhou S *et al.* A distinct bosonic mode in an electron-doped high-transition-temperature superconductor. *Nature* 2007; **450**: 1058–61.
12. Pasupathy AN, Pushp A and Gomes KK *et al.* Electronic origin of the inhomogeneous pairing interaction in the high-T_c superconductor $Bi_2Sr_2CaCu_2O_{8+\delta}$. *Science* 2008; **320**: 196–201.
13. Tonjes WC, Greanya VA and Liu R *et al.* Charge-density-wave mechanism in the 2H-$NbSe_2$ family: angle-resolved photoemission studies. *Phys Rev B* 2001; **63**: 235101.
14. Smith MG, Manthiram A and Zhou J *et al.* Electron-doped superconductivity at 40 K in the infinite-layer compound $Sr_{1-y}Nd_yCuO_2$. *Nature* 1991; **351**: 549–51.
15. Koguchi K, Matsumoto T and Kawai T. Atomic-scale images of the growth surface of $Ca_{1-x}Sr_xCuO_2$ thin films. *Science* 1995; **267**: 71–3.
16. Zhong Y, Fan JQ and Wang RF *et al.* Direct visualization of ambipolar Mott transition in cuprate CuO_2 planes. *Phys Rev Lett* 2020; **125**: 077002.
17. Fan JQ, Wang SZ and Yu XQ *et al.* Molecular beam epitaxy growth and surface structure of $Sr_{1-x}Nd_xCuO_2$ cuprate films. *Phys Rev B* 2020; **101**: 180508 (R).
18. Adachi H, Satoh T and Ichikawa Y *et al.* Superconductivity (Sr, Nd)CuO_y thin films with infinite-layer structure. *Physica C* 1992; **196**: 14–6.
19. Chen CT, Seneor P and Yeh NC *et al.* Strongly correlated *s*-wave superconductivity in the N-type infinite-layer cuprate. *Phys Rev Lett* 2002; **88**: 227002.
20. Harter JW, Maritato L and Shai DE *et al.* Nodeless superconducting phase arising from a strong (π, π) antiferromagnetic phase in the infinite-layer electron-doped $Sr_{1-x}La_xCuO_2$ compound. *Phys Rev Lett* 2012; **109**: 267001.

21. Eschrig M. The effect of collective spin-1 excitations on electronic spectra in high-T_c superconductors. *Adv Phys* 2006; **55**: 47–183.
22. Tajima S, Mizuo Y and Airma T *et al.* Optical-phonon study of single crystals of various layered cuprates and related materials: evidence of unique electron-phonon coupling in the CuO_2 plane. *Phys Rev B* 1991; **43**: 10496–507.
23. Zhou XJ, Cardona M and König W *et al.* Far-infrared reflectance and Raman scattering study of infinite-layer $SrCuO_2$. *Physica C* 1997; **282–7**: 1011–2.
24. Dynes RC, Narayanamurti V and Garno JP. Direct measurement of quasiparticle-lifetime broadening in a strong-coupled superconductor. *Phys Rev Lett* 1978; **41**: 1509–12.
25. Hu C, Zhao J and Gao Q *et al.* Momentum-resolved visualization of electronic evolution in doping a Mott insulator. *Nat Commun* 2021; **12**: 1356.
26. Pan SH, O'Neal JP and Badzey RL *et al.* Microscopic electronic inhomogeneity in the high-T_c superconductor $Bi_2Sr_2CaCu_2O_{8+\delta}$. *Nature* 2001; **413**: 282–5.
27. Cai P, Ruan W and Peng Y *et al.* Visualizing the evolution from the Mott insulator to a charge-ordered insulator in lightly doped cuprates. *Nat Phys* 2016; **12**: 1047–51.
28. Armitage NP, Fournier P and Greene RL. Progress and perspective on electron-doped cuprates. *Rev Mod Phys* 2010; **82**: 2421–87.
29. Hüfner S, Hossain MA and Damascelli A *et al.* Two gaps make a high-temperature superconductor. *Rep Prog Phys* 2008; **71**: 062501.
30. Azuma M, Hiroi Z and Takano M *et al.* Superconductivity at 110 K in the infinite-layer compound $(Sr_{1-x}Ca_x)_{1-y}CuO_2$. *Nature* 1992; **356**: 775–6.
31. Chen CT, Beyer AD and Yeh NC. Effects of compering orders and quantum phase fluctuations on the low-energy excitations and pseudogap phenomena of cuprate superconductors. *Solid State Commun* 2007; **143**: 447–52.
32. Misra S, Oh S and Hornbaker DJ *et al.* Atomic scale imaging and spectroscopy of a CuO_2 plane at the surface of $Bi_2Sr_2CaCu_2O_{8+\delta}$. *Phys Rev Lett* 2002; **89**: 087002.
33. Kitazawa K. Microscopic tunneling spectroscopy on high-temperature superconductors. *Science* 1996; **271**: 313–4.
34. Ren MQ, Han S and Wang SZ *et al.* Direct observation of full-gap superconductivity and pseudogap in two-dimensional fullerides. *Phys Rev Lett* 2020; **124**: 187001.
35. Wang QY, Li Z and Zhang WH *et al.* Interface-induced high-temperature superconductivity in single unit-cell FeSe films on $SrTiO_3$. *Chin Phys Lett* 2012; **29**: 037402.
36. Wen CHP, Xu HC and Chen C *et al.* Anomalous correlation effects and unique phase diagram of electron-doped FeSe revealed by photoemission spectroscopy. *Nat Commun* 2016; **7**: 10840.
37. Zhang SY, Wei T and Guan J *et al.* Enhanced superconducting state in FeSe/$SrTiO_3$ by a dynamical interfacial polaron mechanism. *Phys Rev Lett* 2019; **122**: 066802.
38. Micnas R, Ranninger J and Robaszkiewicz S. Superconductivity in narrow-band systems with local nonretarded attractive interactions. *Rev Mod Phys* 1990; **62**: 113–71.
39. Kresin VZ and Wolf SA. Colloquium: electron-lattice interaction and its impact on high T_c superconductivity. *Rev Mod Phys* 2009; **81**: 481–501.